Research Article

Nonlinear Modeling of Cables with Flexural Stiffness

Walter Lacarbonara[1] and Arnaud Pacitti[2]

[1] *Dipartimento di Ingegneria Strutturale e Geotecnica, Università degli studi di Roma la Sapienza,*
  Via Eudossiana, 00184 Rome, Italy
[2] *Ecole Nationale des Travaux Publics de L'Etat, Laboratoire des Séomatériaux,*
  69120 Vaulx-En-Velin, France

Correspondence should be addressed to Walter Lacarbonara, walter.lacarbonara@uniroma1.it

A geometrically exact formulation of cables suffering axis stretching and flexural curvature is presented. The dynamical formulation is based on nonlinearly viscoelastic constitutive laws for the tension and bending moment with the additional constitutive nonlinearity accounting for the no-compression condition. A continuation method, combined with a mixed finite-difference spatial discretization, is then employed to path-follow the static responses of cables subject to forces or support displacements. These computations, conducted in the quasistatic regime, are based on cables with linearly elastic material behaviors, whereas the nonlinearity is in the geometric stiffness terms and the no-compression behavior. The finite-difference results have been confirmed employing a weak formulation based on quadratic Lagrangian finite elements. The influence of the flexural stiffness on the nonlinear static responses is assessed comparing the results with those obtained for purely extensible cables. The properties of the frequencies of the linear normal modes of cables with flexural stiffness are also investigated and compared with those of purely extensible cables.

1. Introduction

Cables are used in a variety of engineering applications such as in suspension or cable-stayed bridges, power transmission lines, moorings in ocean engineering, or in aerospace deployable structures. Cables are effectively employed in long-span structures because they can be easily engineered and are light-weight structural elements with an outstanding stiffness in the axial direction and a significantly high strength. However, they do possess limitations due to the lack of out-of-plane stiffness and very light damping that make them often prone to large-amplitude

vibrations. Another serious limitation is that they cannot resist compression, therefore, they are always prestressed to resist actions that may produce compression although under severe dynamic excitations, the low-tension regime is barely unavoidable.

Although a number of works have addressed the problem of modeling the flexural stiffness in cables, only a few works deal with nonlinear vibrations of general cables in low-tension regimes. Most of them consider nonlinear vibrations of shallow/taut cables, including also multiple resonances [1–4]. In [5, 6], a geometrically exact nonlinear model of linearly elastic nonshallow cables was proposed, and the nonlinear modal characteristics of the free planar motions were investigated neglecting flexural stiffness as it is commonly done in the literature. In fact, flexural stiffness appears in modeling cables only when the loosening effect is considered. When the excitation levels are high, the loss of tension can be such that the cable suffers local loosening in those segments where the overall tension vanishes and, as a result, the cable cannot locally sustain loads unless its flexural load-carrying capability is considered. Most of the times, the flexural rigidity and damping are considered in a cable model to overcome numerical divergence problems when loosening appears. For instance, when dealing with the dynamics of submerged cables, some works focus on a general mechanical formulation for the cable equations (e.g., [7–9]); such equations of motion are then solved by direct integration schemes. Other works focus on the derivation or modification of finite-element solution models (e.g., [10]), or even in simplified solution models such as the lumped mass approach of Chai et al. [11]. Similarly, Wu et al. [12–15] used a model of cables that includes the linear flexural stiffness contribution, and an approximate strain-displacement relationship for the elongation, to describe nonlinear vibrations of cables suffering loosening. Moreover, with the proposed model, the effects of loosening on the nonlinear parametric responses of taut cables subject to periodic horizontal displacements of the supports were investigated.

However, the effects of flexural rigidity and viscoelasticity on the nonlinear dynamics of cables have not been thoroughly investigated, especially when loosening appears. Furthermore, the flexural stiffness has a critical role in stock-bridge dampers used to dissipate energy. There is a need to have a reliable and accurate mechanical model of cables to assess the global load-carrying capability under these conditions. There are only a few studies addressing this challenging modeling problem and they are often based on ad hoc approximations that limit the physically meaningful dynamic regimes.

In this paper, a nonlinear geometrically exact formulation of cables undergoing axis stretching and flexural curvature, incorporating a nonlinearly viscoelastic constitutive law and the no-compression condition, is first presented. The derivation of the mechanical model is extensively inspired by the seminal work of Antman [16]. Thereafter, the linearization and the ensuing eigenvalue problem are addressed. Then, the finite-difference computational scheme is illustrated. Meaningful static responses of cables subject to various loading paths—support displacements or forces—are investigated in both cable models, here considered, the model with flexural stiffness and that without flexural resistance.

2. Mechanical formulation for cables with flexural stiffness

In this section, we illustrate the geometrically exact formulation of the equations of motion of cables suffering axis stretching and bending curvature [16]. Shear deformations are not considered. Moreover, a planar kinematic model is discussed neglecting out-of-plane bending
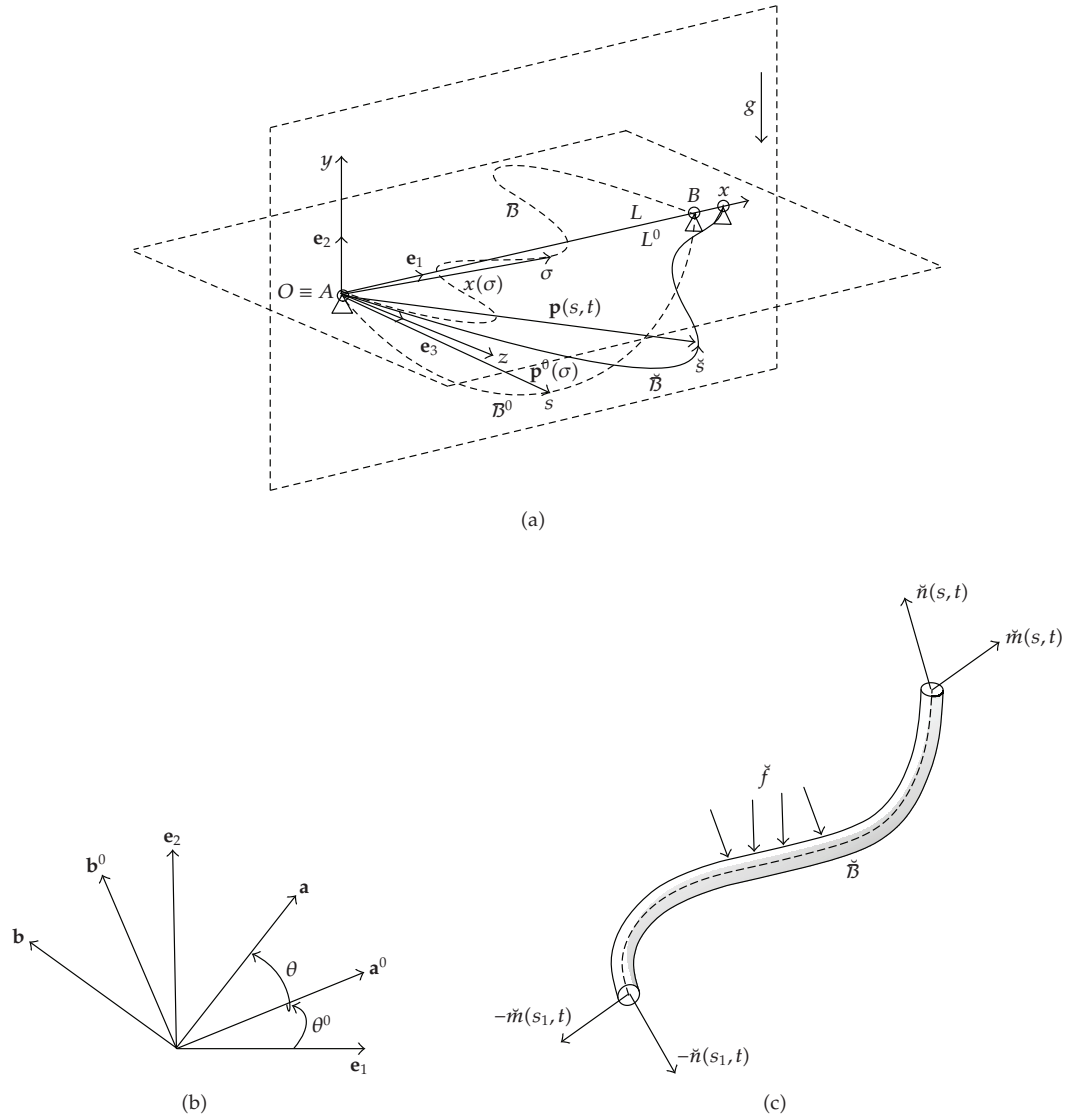
Figure 1: Stress-free configuration $\mathcal{B}$, prestressed configuration $\mathcal{B}^0$, and actual configuration $\breve{\mathcal{B}}$ (top). Unit vectors and rotations of the plane kinematics (bottom left) and internal/external forces in the cable (bottom right).

and torsion. The prestressed equilibrium is first discussed, then the dynamics around it are described in the kinematic, dynamic, and constitutive aspects.

2.1. The prestressed cable

The cable is stress-free in the configuration $\mathcal{B}$ (Figure 1(a)). This configuration can be any arbitrary configuration assumed by the cable, for example, on a frictionless horizontal plane

when it is not subject to forces besides the gravity force. In this state, the internal stresses are expected to be practically vanishing. In particular, in Figure 1(a), $\mathcal{B}$ represents any reference line along the cable in the stress-free configuration (e.g., the centroidal line) and L is its undeformed length. Further, we let the arc length, denoted σ, be the coordinate identifying the material sections of the cable. We consider the fixed Cartesian reference frame $(O, \mathbf{e}_1, \mathbf{e}_3, \mathbf{e}_3)$ shown in Figure 1(a). When the cable ends are fixed to two points, A and B, and the cable is let free to hang under the action of gravity, it occupies an equilibrium configuration, here denoted $\mathcal{B}^0$, and considered as the reference configuration for the subsequent dynamic problem. The arc length in the configuration $\mathcal{B}^0$ is denoted s. Let the position vector of the material point P^0 of the cable in the reference configuration $\mathcal{B}^0$ be $\mathbf{p}^0$. Among the different parameterizations for $\mathbf{p}^0$, we employ σ, and let the Cartesian representation of $\mathbf{p}^0$ be $\mathbf{p}^0(\sigma) := x(\sigma)\mathbf{e}_1 + y(\sigma)\mathbf{e}_2$.

The cable stretch is then simply defined as

$$\mathbf{p}_\sigma^0(\sigma) = v^0(\sigma)\mathbf{a}^0(\sigma), \tag{2.1}$$

where $\mathbf{a}^0$ is the unit vector in the tangential direction to $\mathcal{B}^0$; the subscript here and henceforth will denote partial differentiation with respect to the indicated variable. Consequently, the stretch is

$$v^0(\sigma) = \left| \mathbf{p}_\sigma(\sigma) \right| = \frac{ds}{d\sigma}. \tag{2.2}$$

We suppose that the cable flexural rigidity is negligible in the equilibrium $\mathcal{B}^0$ under its own weight, hence the stress vector representing the contact force that the cable segment $\sigma > \sigma_1$ exerts on the cable segment $\sigma < \sigma_1$ through the material section at σ_1 has a resultant (integrated on the domain representing the deformed cable material section) referred to as contact force and denoted $\mathbf{n}^0$. On the other hand, the resultant moment is vanishing. This assumption holds true because under its own weight (uniformly distributed), the cable will assume a funicular configuration having the tension carrying the weight.

By denoting $\mathbf{f}^0$, the force per unit reference length σ, the local form of the balance of linear and angular momentum can be written as

$$\mathbf{n}_\sigma^0(\sigma) + \mathbf{f}^0(\sigma) = \mathbf{o}, \qquad \mathbf{p}_\sigma^0(\sigma) \times \mathbf{n}^0(\sigma) = \mathbf{o}. \tag{2.3}$$

The second part of equation (2.3) implies that $\mathbf{n}^0$ is in the same direction as $\mathbf{p}_\sigma^0 = v^0 \mathbf{a}^0$, that is, in the direction of the tangent to the deformed configuration $\mathcal{B}^0$; hence, $\mathbf{n}^0(\sigma) = N^0(\sigma)\mathbf{a}^0(\sigma)$, where N^0 denotes the magnitude of the contact force, commonly referred to as the tension. Moreover, the unit vector $\mathbf{a}^0$ can be expressed as

$$\mathbf{a}^0 = \frac{\mathbf{p}_\sigma^0}{\left|\mathbf{p}_\sigma^0\right|} = \frac{\mathbf{p}_\sigma^0}{v^0}. \tag{2.4}$$

The final balance equation is then rewritten as

$$\left[N^0(\sigma)\mathbf{a}^0(\sigma) \right]_\sigma + \mathbf{f}^0 = \mathbf{o}. \tag{2.5}$$

The constitutive law relating the tension N^0 to the stretch v^0 is introduced in the form

$$N^0(\sigma) = \widehat{N}^0(v^0, \sigma). \tag{2.6}$$

A few restrictions are imposed on $\widehat{N}^0$ as $\widehat{N}^0(\nu^0 = 1, \sigma) = 0$, $\widehat{N}_\nu > 0$. Moreover, for materials strong in resisting tension, we may require $\widehat{N}^0 \to \infty$ as $\nu^0 \to \infty$.

The governing equilibrium equation is obtained substituting (2.6) into (2.5). The equilibrium equation can be projected into the local basis $\{\mathbf{a}^0, \mathbf{b}^0, \mathbf{c}^0\}$ (with $\mathbf{c}^0 \equiv \mathbf{e}_3$) or the fixed basis $(\mathbf{e}_1, \mathbf{e}_2, \mathbf{e}_3)$. Using the local basis, accounting for $(\mathbf{a}^0)_\sigma = \nu^0 \mu^0 \mathbf{b}^0$, with $\mu^0 = \theta_s^0$ (the geometric curvature of $\mathcal{B}^0$), and letting $\mathbf{f}^0 = f_1^0 \mathbf{a}^0 + f_2^0 \mathbf{b}^0$ yield

$$\widehat{N}_\sigma^0 + f_1^0 = 0, \qquad \nu^0 \mu^0 \widehat{N}^0 + f_2^0 = 0. \tag{2.7}$$

On the other hand, projecting (2.5) into the fixed basis $(\mathbf{e}_1, \mathbf{e}_2, \mathbf{e}_3)$ and accounting for $\mathbf{a}^0 = \cos\theta^0 \mathbf{e}_1 + \sin\theta^0 \mathbf{e}_2$ and $\mathbf{b}^0 = -\sin\theta^0 \mathbf{e}_1 + \cos\theta^0 \mathbf{e}_2$ yield

$$\left[\widehat{N}^0 \cos\theta^0\right]_\sigma + b_1^0 = 0, \qquad \left[\widehat{N}^0 \sin\theta^0\right]_\sigma + b_2^0 = 0, \tag{2.8}$$

where $\mathbf{f}^0 = b_1^0 \mathbf{e}_1 + b_2^0 \mathbf{e}_2$.

The relationships between $(\cos\theta^0, \sin\theta^0)$ and $(x_\sigma, y_\sigma, \nu^0)$ can be obtained considering $\mathbf{p}_\sigma^0 = x_\sigma \mathbf{e}_1 + y_\sigma \mathbf{e}_2$ and $\mathbf{a}^0 = \cos\theta^0 \mathbf{e}_1 + \sin\theta^0 \mathbf{e}_2$, that is,

$$\cos\theta^0 = \frac{x_\sigma}{\nu^0}, \qquad \sin\theta^0 = \frac{y_\sigma}{\nu^0}. \tag{2.9}$$

From the fundamental trigonometric identity $(\sin^2\theta^0 + \cos^2\theta^0 = 1)$, the stretch becomes $\nu^0 = \sqrt{x_\sigma^2 + y_\sigma^2}$. The solution for the static configuration $\mathcal{B}^0$ under the dead loads and, more specifically, under the action of gravity, is described in the Appendix. We will discuss cables suspended from two points at the same level (horizontal cables) or at different levels (inclined cables).

2.2. The dynamic incremental problem

The transformation from the static configuration $\mathcal{B}^0$ to the current configuration $\breve{\mathcal{B}}$ is illustrated next. We let $\mathbf{p}(s, t) = \mathbf{p}^0(s) + \mathbf{u}(s, t)$ be the position vector of the point of the cable in $\breve{\mathcal{B}}$ and let the arc length in $\breve{\mathcal{B}}$ be denoted š. We will treat, to start with, the planar problem (see Figure 1(b)). Hence, let $\mathbf{b}(s, t)$ be the unit vector giving the orientation of the cable cross-section in $\breve{\mathcal{B}}$ so that the cable-fixed basis in $\breve{\mathcal{B}}$ is $(\mathbf{a}(s, t), \mathbf{b}(s, t))$ and θ denotes the rotation angle from $(\mathbf{a}^0, \mathbf{b}^0)$ to $(\mathbf{a}, \mathbf{b})$. Therefore, the angle that $\mathbf{a}$ makes with $\mathbf{e}_1$ is $\breve{\theta} = \theta^0 + \theta$.

The cable total stretch is obtained, by enforcing the shear strain to vanish, as $\mathbf{p}_\sigma = \breve{\nu}\mathbf{a}$, where $\breve{\nu} = d\check{s}/d\sigma = \nu\nu^0$, that is, the product of the initial stretch and the incremental stretch ν. To calculate the cable incremental stretch ν that arises in the motion from $\mathcal{B}^0$ to $\breve{\mathcal{B}}$, we consider $\mathbf{p}_s = \nu\mathbf{a}$. Then, by letting $\mathbf{u}(s, t) = u(s, t)\mathbf{a}^0(s, t) + v(s, t)\mathbf{b}^0$ represent the displacement vector from $\mathcal{B}^0$ to $\breve{\mathcal{B}}$, the position vector is $\mathbf{p} = \mathbf{p}^0 + \mathbf{u}$ and its gradient becomes $\mathbf{p}_s = \mathbf{p}_s^0 + \mathbf{u}_s = (1 + u_s - \mu^0 v)\mathbf{a}^0 + (v_s + \mu^0 u)\mathbf{b}^0$. Consequently,

$$\nu = \sqrt{\left(1 + u_s - \mu^0 v\right)^2 + \left(v_s + \mu^0 u\right)^2}, \tag{2.10}$$

$$\mathbf{a} = \frac{\left(1 + u_s - \mu^0 v\right)\mathbf{a}^0 + \left(v_s + \mu^0 u\right)\mathbf{b}^0}{\nu}. \tag{2.11}$$

Moreover,

$$\sin\theta = \frac{\mathbf{p}_s \cdot \mathbf{b}^0}{\nu} = \frac{v_s + \mu^0 u}{\nu}, \qquad \cos\theta = \frac{\mathbf{p}_s \cdot \mathbf{a}^0}{\nu} = \frac{1 + u_s - \mu^0 v}{\nu}. \tag{2.12}$$

Dividing the left- and right-hand sides of the two preceding equations and considering the inverse tangent function yield the incremental angle θ as

$$\theta = \tan^{-1}\left(\frac{v_s + \mu^0 u}{1 + u_s - \mu^0 v}\right). \tag{2.13}$$

Therefore, the flexural curvature μ is

$$\mu = \frac{d\theta}{ds} = \frac{1}{\nu^2}\left[(v_{ss} + (\mu^0 u)_s)(1 + u_s - \mu^0 v) - (u_{ss} - (\mu^0 v)_s)(v_s + \mu^0 u)\right]. \tag{2.14}$$

The presentation of the kinematic model is complete once the boundary conditions are prescribed. For generality, we consider the cable supports lying in the $(\mathbf{e}_1, \mathbf{e}_2)$-plane and being placed at different levels and immovable under the dead loads, $\mathbf{x}(0) = \mathbf{p}^0(0) = \mathbf{o}$, $\mathbf{x}(L) = \mathbf{p}^0(L) = \ell\mathbf{e}_1 + h\mathbf{e}_2$. On the contrary, the supports prescribe some smooth motions during the dynamic change of configuration from $\mathcal{B}^0$ to $\breve{\mathcal{B}}$. Hence, the time-dependent boundary conditions become

$$\mathbf{p}(0,t) = \mathbf{u}_A(t) = u_A(t)\mathbf{e}_2, \qquad \mathbf{p}(L,t) = \mathbf{p}^0(L) + \mathbf{u}_B(t) = (l + u_B(t))\mathbf{e}_1 + h\mathbf{e}_2. \tag{2.15}$$

Next, the dynamical aspects of the problem are discussed. We let $\breve{\mathbf{n}} = \breve{N}\mathbf{a} + \breve{H}\mathbf{b}$ be the contact force in the cable at $\breve{s}$, let $\mathbf{f}$ be the incremental external forces such that $\breve{\mathbf{f}}(s,t) = \mathbf{f}^0(s) + \mathbf{f}(s,t)$ indicates the total external force density acting on the cable (per unit reference length s), and let $\breve{\mathbf{m}}$ be the total flexural moment of the cable at $\breve{s}$. Please note that here $\mathbf{f}^0(s)$ denotes the force acting in $\mathcal{B}^0$, however, referred, for convenience, to the unit reference length s instead of σ. In the current configuration $\breve{\mathcal{B}}$, the local form of the balance of linear and angular momentum requires

$$\breve{\mathbf{n}}_s(s,t) + \breve{\mathbf{f}}(s,t) = \rho A^0 \mathbf{p}_{tt}(s,t),$$

$$\breve{\mathbf{m}}_s(s,t) + \mathbf{p}_s(s,t) \times \breve{\mathbf{n}}(s,t) = \mathbf{o}. \tag{2.16}$$

By accounting for $\mathbf{p}_s(s,t) = \nu\mathbf{a}$, the balance of angular momentum yields

$$\breve{\mathbf{m}}_s + \nu\breve{H}\mathbf{e}_3 = \mathbf{o}. \tag{2.17}$$

Further, let N and H be the incremental axial and shear forces such that $\breve{N} = N^0 + N$ and $\breve{H} \equiv H$, since the reactive shear force H^0 in $\mathcal{B}^0$ is zero. Hence, the total contact force is $\breve{\mathbf{n}} = (N^0 + N)\mathbf{a} + H\mathbf{b}$. Similarly, $\mathbf{m}$ is the incremental flexural moment coinciding with the total flexural moment since the cable flexural stiffness is neglected in the initial static configuration, therefore, $\breve{\mathbf{m}} = \mathbf{m}$. Since $\mathbf{m} = M\mathbf{e}_3$, (2.17), solved for H, yields the shear force as $H = -M_s/\nu$. We can rewrite the equation of motion (2.16) as

$$\left(\breve{N}\mathbf{a} - \frac{M_s}{\nu}\mathbf{b}\right)_s + \mathbf{f}^0 + \mathbf{f} = \rho A^0 \mathbf{p}_{tt}. \tag{2.18}$$

By considering the equilibrium in $\mathcal{B}^0$, $(N^0\mathbf{a}^0)_s + \mathbf{f}^0 = \mathbf{o}$, and by letting $\check{N}\mathbf{a} = N^0\mathbf{a}^0 + N^0(\mathbf{a} - \mathbf{a}^0) + N\mathbf{a}$, the equation of motion (2.18) becomes

$$(N\mathbf{a})_s + \left[N^0(\mathbf{a} - \mathbf{a}^0)\right]_s - \left(\frac{M_s}{v}\mathbf{b}\right)_s + \mathbf{f} = \rho A^0 \mathbf{p}_{tt}. \tag{2.19}$$

The componential form of (2.19) in the cable-fixed basis $(\mathbf{a}^0, \mathbf{b}^0)$ becomes

$$\left[(N^0 + N)_s + \frac{M_s}{v}(\mu^0 + \mu)\right]\cos\theta - \left[(N^0 + N)(\mu^0 + \mu) - \left(\frac{M_s}{v}\right)_s\right]\sin\theta - N_s^0 + f_1 = \rho A^0 u_{tt}, \tag{2.20}$$

$$\left[(N^0 + N)_s + \frac{M_s}{v}(\mu^0 + \mu)\right]\sin\theta + \left[(N^0 + N)(\mu^0 + \mu) - \left(\frac{M_s}{v}\right)_s\right]\cos\theta - \mu^0 N^0 + f_2 = \rho A^0 v_{tt}, \tag{2.21}$$

where $\mathbf{f} = f_1\mathbf{a}^0 + f_2\mathbf{b}^0$, $\rho A^0\mathbf{p}_{tt} = \rho A^0 u_{tt}\mathbf{a}^0 + \rho A^0 v_{tt}\mathbf{b}^0$.

Suitable nonlinearly viscoelastic constitutive laws for the tension N and the bending moment M are given in the form

$$N(s,t) = \widehat{N}(v, v_t, s), \quad \text{iff } \check{v} = v^0 v > 1,$$

$$M(s,t) = \widehat{M}(\mu, \mu_t, s). \tag{2.22}$$

For materials whose constitutive behavior is linearly viscoelastic also at large strains and strain rates, the linearized version of the nonlinear constitutive laws can be expressed in the form

$$\widehat{N} = EA(v - 1) + (\widehat{N}_{\dot{v}})v_t, \quad \text{iff } \check{v} = v^0 v > 1,$$

$$\widehat{M} = EJ\mu + (\widehat{M}_{\dot{\mu}})\mu_t. \tag{2.23}$$

The constitutive law for $\check{N}$ is nonlinear in the sense that, because the cable cannot resist compression, in those segments of the cable where $\check{v} \le 1$, the total tension vanishes, that is, $\check{N} = N^0 + \widehat{N} = 0$. When a total loss of tension occurs, the cable does not undergo any local length changes, hence letting $\check{v} = v^0 v = 1$ yields the incremental stretching in terms of the prestretching, that is, $v = 1/v^0$. In the corresponding cable subdomains, the balance equations are accordingly modified putting $\check{N} = 0$ and $\check{v} = 1$. Hence,

$$-\left[N^0\mathbf{a}^0\right]_s - \left(\frac{M_s}{v}\mathbf{b}\right)_s + \mathbf{f} = \rho A^0\mathbf{p}_{tt}. \tag{2.24}$$

The strain-displacement relationships (2.10) and (2.14) are substituted into the constitutive equations (2.22) and these, in turn, are substituted, along with (2.12), into the equations of (2.20) and (2.21) delivering the final governing equations of motion in the unknown displacements u and v.

We finally nondimensionalize the equations of motion introducing the followin nondimensional quantities:

$$s^* = \frac{s}{\ell}, \qquad u^* = \frac{u}{\ell}, \qquad v^* = \frac{v}{\ell}, \qquad t^* = \sqrt{\frac{H^0}{\rho A^0 \ell^2}} t,$$

$$\mu^{0*} = \ell \mu^0, \qquad \mu^* = l\mu, \qquad f^* = \frac{\ell f}{H^0}, \qquad k = \frac{EA^0}{H^0},$$

$$N^{0*} = \frac{N^0}{H^0}, \qquad N^* = \frac{N}{H^0}, \qquad M^* = \frac{M}{\ell H^0}, \qquad \Lambda = \frac{EJ^0}{\ell^2 H^0}. \tag{2.25}$$

By dropping the star for notational simplicity and by neglecting the dissipative parts of the incremental dynamic tension and moment, the nondimensional equations of motion, for linearly elastic cables, become

$$N_s^0 \left[\frac{1 + u_s - \mu^0 v}{v} - 1 \right] - N^0 (\mu^0 + \mu) \left(\frac{v_s + \mu^0 u}{v} \right)$$

$$+ k \left[v_s \frac{1 + u_s - \mu^0 v}{v} - (v - 1)(\mu^0 + \mu) \left(\frac{v_s + \mu^0 u}{v} \right) \right] \tag{2.26}$$

$$+ \Lambda \left[(\mu^0 + \mu) \left(\frac{\mu_s}{v} \right) \left(\frac{1 + u_s - \mu^0 v}{v} \right) + \left(\frac{\mu_{ss}}{v} - \frac{v_s \mu_s}{v^2} \right) \left(\frac{v_s + \mu^0 u}{v} \right) \right] + f_1 = u_{tt},$$

$$N_s^0 \left[\frac{v_s + \mu^0 u}{v} \right] + N^0 \left[(\mu^0 + \mu) \frac{1 + u_s - \mu^0 v}{v^2} - \mu^0 \right]$$

$$+ k \left[(v - 1)(\mu^0 + \mu) \left(\frac{1 + u_s - \mu^0 v}{v} + v_s \frac{v_s + \mu^0 u}{v} \right) \right] \tag{2.27}$$

$$+ \Lambda \left[(\mu^0 + \mu) \left(\frac{\mu_s}{v} \right) \left(\frac{v_s + \mu^0 u}{v} \right) + \left(\frac{\mu_s v_s}{v^2} - \frac{\mu_{ss}}{v} \right) \left(\frac{1 + u_s - \mu^0 v}{v} \right) \right] + f_2 = v_{tt},$$

where the stretch v and the curvature μ are expressed by (2.10) and (2.14). On the other hand, the equations of motion in the case of a total decompression, with a linearly elastic material, become

$$v^{0^2}(\mu^0 + \mu)(1 + u_s - \mu^0 v)(\Lambda \mu)_s + v^0 (v_s + \mu^0 u) \left[v^0 (\Lambda \mu)_s \right]_s - N_s^0 + f_1 = u_{tt},$$

$$v^{0^2}(\mu^0 + \mu)(v_s + \mu^0 u)(\Lambda \mu)_s - v^0 (1 + u_s - \mu^0 v) \left[v^0 (\Lambda \mu)_s \right]_s - \mu^0 N^0 + f_2 = v_{tt}. \tag{2.28}$$

3. The linearization and vibration eigenvalue problem

The linearization of (2.19) can be systematically obtained once we introduce a small parameter, denoted ϵ, which suitably quantifies the deviations from the prestressed configuration $\mathcal{B}^0$. We

neglect the dissipative parts of the tension and bending moment and the forcing. We assume $v = v(\epsilon)$, $\mu = \mu(\epsilon)$, $\widehat{N} = \widehat{N}(v(\epsilon))$, $\widehat{M} = \widehat{M}(\mu(\epsilon))$, $\mathbf{u}_s = \mathbf{u}_s(\epsilon)$, $\mathbf{a} = \mathbf{a}(\epsilon)$ as continuously differentiable functions of ϵ. Further,

$$v(0) = 1, \qquad \mu(0) = 0, \qquad \widehat{N}(v(0)) = 0, \qquad \widehat{M}(\mu(0)) = 0,$$

$$\mathbf{a}(0) = \mathbf{a}^0, \qquad \mathbf{b}(0) = \mathbf{b}^0, \qquad \mathbf{u}_s(0) = \mathbf{o}.$$
(3.1)

Therefore, the elastic parts of the tension and flexural moment can be expanded in series of ϵ as

$$\widehat{N}(v(\epsilon))\mathbf{a}(\epsilon) = \epsilon EA^0 v_1 \mathbf{a}^0 + O(\epsilon^2), \qquad \frac{\widehat{M}(\mu(\epsilon))_s}{v(\epsilon)}\mathbf{b}(\epsilon) = \epsilon (EJ^0 \mu_1)_s \mathbf{b}^0 + O(\epsilon^2),$$
(3.2)

where $v_1 = v_\epsilon(0)$ and $\mu_1 = \mu_\epsilon(0)$ denote the first-order part of the stretch and the curvature (i.e., containing only linear terms in $\mathbf{u}_s$). On the other hand, the geometric part of the internal force, expanded in series of ϵ, yields $N^0(\mathbf{a}(\epsilon) - \mathbf{a}^0) = N^0 \mathbf{a}_1 + O(\epsilon^2)$, where $\mathbf{a}_1 = \mathbf{a}_\epsilon(0)$ is the first-order deviation of $\mathbf{a}$ from $\mathbf{a}^0$. By retaining only first-order terms in the expansion of the equations of motion, we obtain the linearized equations of motion

$$(EA^0 v_1 \mathbf{a}^0)_s + (N^0 \mathbf{a}_1)_s - ((EJ^0 \mu_1)_s \mathbf{b}^0)_s = \rho A^0 \mathbf{u}_{tt}.$$
(3.3)

To calculate v_1, μ_1, and $\mathbf{a}_1$, we consider (2.10), (2.14), and (2.11), and by differentiating them with respect to ϵ and by setting $\epsilon = 0$, we obtain

$$v_1 = u_s - \mu^0 v, \qquad \mu_1 = v_{ss} + \mu_s^0 u + \mu^0 u_s, \qquad \mathbf{a}_1 = (v_s + \mu^0 u)\mathbf{b}^0.$$
(3.4)

The first-order variation of $\mathbf{a}$ can be alternatively obtained from $\mathbf{a} = \cos\theta(\epsilon)\mathbf{a}^0 + \sin\theta(\epsilon)\mathbf{b}^0 = \mathbf{a}^0 + \epsilon\theta_1 \mathbf{b}^0 + O(\epsilon^2)$, where the first-order variation of θ, given by (2.13), is $\theta_1 = v_s + \mu^0 u$. Therefore,

$$\left[EA^0(u_s - \mu^0 v)\right]_s + \mu^0\left[EJ^0(v_{ss} + \mu_s^0 u + \mu^0 u_s)\right]_s - \mu^0 N^0(v_s + \mu^0 u) = \rho A^0 u_{tt},$$

$$\mu^0\left[EA^0(u_s - \mu^0 v)\right] - \left[EJ^0(v_{ss} + \mu_s^0 u + \mu^0 u_s)\right]_{ss} + N_s^0(v_s + \mu^0 u) + N^0(v_s + \mu^0 u)_s = \rho A^0 v_{tt}.$$
(3.5)

In nondimensional form,

$$\left[k(u_s - \mu^0 v)\right]_s + \mu^0\left[\Lambda(v_{ss} + \mu_s^0 u + \mu^0 u_s)\right]_s - \mu^0 N^0(v_s + \mu^0 u) = u_{tt},$$
(3.6)

$$\mu^0 k(u_s - \mu^0 v) - \left[\Lambda(v_{ss} + \mu_s^0 u + \mu^0 u_s)\right]_{ss} + N_s^0(v_s + \mu^0 u) + N^0(v_{ss} + \mu_s^0 u + \mu^0 u_s) = v_{tt}.$$

3.1. The cable elastogeometric parameters

The linear as well as nonlinear free motions of linearly elastic nonshallow cables without flexural stiffness depend on two parameters [5] related to their geometric and elastic stiffnesses, namely, γ and k, contrary to shallow cables [1] whose linear motions depend solely

on Irvine's elastogeometric parameter λ. Irvine's parameter combines the two characteristic parameters of nonshallow cables according to $\lambda^2 := \gamma^2 k/\eta^e$ with $\eta^e = \int_0^{\eta^0} \sec^2 \theta^0 ds$, $\eta^0 = L/\ell$. For cables suffering stretching and bending in the plane and made of a linearly elastic material, the independent governing parameters are three, namely, (γ, k, Λ) or, equivalently, $(\gamma, \lambda, \Lambda)$.

We discuss in more detail the cable parameters pointing out their mechanical significance and pertinent ranges of variation. The region of admissible elastic stiffness k in the (γ, λ)-plane was discussed in [5] considering the isostiffness curves according to the definition of Irvine's parameter. The boundaries of the admissible region correspond to $k_1 = 5 \cdot 10^2$ and $k_3 = 5 \cdot 10^4$, respectively. These values were determined considering that $k = E/S^0$ and $S^0 = H^0/A^0$ denotes the engineering tensile stress at the mid-span section. Hence, the minimum k_1 is attained when S^0 is maximum, here taken as the yielding tensile strength S^y. Because typical working tensile stresses are around 5–10% of S^y, a reasonable value of k is of the order of 10^3. However, by considering lower tensile stresses in the static configuration, values of k of the order of 10^4 can be reasonably reached.

By assuming a typical circular cross-section, $J^0 = (A^0)^2/(4\pi)$, hence the nondimensional flexural stiffness becomes $\Lambda = kA^0/(4\pi\ell^2)$. Further, it is $\gamma = \rho g\ell/S^0$ and $k = E/S^0$. Hence, by considering the following as design data: (i) the sag ℓ, (ii) the material properties (ρ, E), and (iii) the working tensile stress S^0, the parameters γ and k (or λ) are accordingly determined and are independent of A^0 whereas Λ depends on k, ℓ, and A^0. Therefore, considering iso-k curves, the nondimensional flexural stiffness parameter Λ remains constant only if the cable cross-sectional areas do not vary.

4. Computational scheme: finite-difference versus finite elements

We employ a finite-difference discretization method to path-follow the nonlinear static solutions of (2.26) and (2.27) with f_1 and f_2 being time-independent and being applied through a loading device with a sufficiently slow rate, that is, in a quasistatic fashion. The boundary conditions at A and B prescribe the displacements and the bending moments. In particular, the six boundary conditions are as follows:

$$u(0) = u_A, \qquad v(0) = v_A, \qquad u(\eta^0) = u_B, \qquad v(\eta^0) = v_B, \qquad M(0) = M(\eta^0) = 0. \quad (4.1)$$

By considering a grid with n points including the boundary points A and B, the interior points are $n - 2$. At the interior points, we enforce the two balance equations, with an ensuing number of $2(n - 2)$ field equations. Overall, the number of equations is $2(n + 1)$. If the problem is fully formulated in the displacement components (u, v), then the unknowns would be $2n$ leading to an overconstrained system of nonlinear equations. The problem is circumvented by employing a standard mixed approach (in the sense that it is neither the displacement nor the force method) consisting in taking as unknowns the displacement (u, v) and the bending moment M resulting into $3n$ unknowns. The bending moment, treated as unknown in the balance equations, has to satisfy the constitutive equation which is added explicitly as an independent equation. Therefore, the overall number of equations comprises the $3(n - 2)$ field equations to which the six boundary conditions are to be added, resulting into a system of $3n$ equations in $3n$ unknowns.

Therefore, the field equations read

$$\left[N_s^0 + (k(v-1))_s + \frac{M_s}{v}(\mu^0 + \mu)\right]\cos\theta$$

$$-\left[(N^0 + k(v-1))(\mu^0 + \mu) - \left(\frac{M_s}{v}\right)_s\right]\sin\theta - N_s^0 + f_1 = 0,$$

$$\left[N_s^0 + (k(v-1))_s + \frac{M_s}{v}(\mu^0 + \mu)\right]\sin\theta \tag{4.2}$$

$$+\left[(N^0 + k(v-1))(\mu^0 + \mu) - \left(\frac{M_s}{v}\right)_s\right]\cos\theta - \mu^0 N^0 + f_2 = 0,$$

$$M - \Lambda\frac{1}{v^2}\left[(v_{ss} + (\mu^0 u)_s)(1 + u_s - \mu^0 v) - (u_{ss} - (\mu^0 v)_s)(v_s + \mu^0 u)\right] = 0.$$

To enhance the accuracy of the finite-difference scheme, we employed a five-point scheme [17] based on an equidistant point grid which can be written, considering the first-order space derivative, as follows:

$$\frac{1}{12 \times \Delta}\begin{bmatrix} -25 & 48 & -36 & 16 & -3 \\ -3 & -10 & 18 & -6 & 1 \\ 1 & -8 & 0 & 8 & -1 \\ -1 & 6 & -18 & 10 & 3 \\ 3 & -16 & 36 & -48 & 25 \end{bmatrix}, \tag{4.3}$$

where $\Delta = s_i - s_{i-1}$ denotes the distance between two adjacent points of the grid.

For the chosen n-point grid, we have $3n$ equations, each expressed as a function of

$$\left[(u_{i-2}, u_{i-1}, u_i, u_{i+1}, u_{i+2}), (v_{i-2}, v_{i-1}, v_i, v_{i+1}, v_{i+2}), (M_{i-2}, M_{i-1}, M_i, M_{i+1}, M_{i+2})\right] \tag{4.4}$$

and the external force term f_i, where i is the index associated to the grid point. Out of the six boundary conditions, four equations are kinematic, namely, $u_0 = u_A$, $u_n = u_B$, $v_0 = v_A$, $v_n = v_B$, two of them are mechanical, $M_0 = M_n = 0$. Further, mention must be made of the fact that the discretization at the two points adjacent to the boundary points is not clearly centered.

The problem is solved step-by-step employing a zeroth-order path-following scheme where the Newton-Raphson iterative scheme is exploited at each load step to find the new solution point. The procedure was implemented in MATHEMATICA [18]. At each load step, the external force is increased by Δf_i and the solution point of the preceding step is used as the initial guess in the updated load step; in this sense, the continuation procedure is based on a zeroth-order predictor. At the end of each load step, the determined solution is expected to satisfy the balance equations ensuring that the pointwise remainders are below a prescribed numerical tolerance.

The same analyses have been conducted employing COMSOL [19]. COMSOL Multiphysics allows to approximate partial-differential equations of various kinds via a finite element procedure. The number of quadratic Lagrangian finite elements was set to 7680 in all calculations, for a total number of 76 805 degrees of freedom, and the tolerance was fixed to 10^{-6}. The high number of finite elements was not strictly needed, it was chosen in all calculations for accuracy reasons. A close agreement between the finite difference-based (with number of grid points greater than or equal to 30) and finite element-based results has been found and it is such that only the outcomes of COMSOL are reported next.

5. Illustrative examples of nonlinear static responses

It is of interest to investigate into the differences exhibited by the nonlinear structural responses of cables possessing flexural stiffness and those of cables whose flexural stiffness is neglected. The objective is to assess the extent of the bending stiffness contribution within the context of static loading processes. It is clear, however, that the most significant effects are expected to be exhibited in dynamic regimes, especially near resonances and instabilities.

In this section, we present some illustrative examples of nonlinear responses to three different loading scenarios. All loading cases are selected so as to induce a gradual loss of tension that enhances the bending moment contribution. The first case features a horizontal cable, lying under its own weight between two points at the same level. A constant uniformly distributed vertical upward load is applied over a central region of the cable. In the other two cases, the loading path is a prescribed incremental displacement of the right support to the left so as to loosen the cable. We consider both a horizontal and an inclined cable.

Two different cables are considered in the numerical computations and they have the following nondimensional governing parameters: $\eta^0 = 1.09615$, $\gamma = 1.5$, $k = 1.10 \cdot 10^4$, $\Lambda = 4.43 \cdot 10^{-4}$, for the horizontal cable, and $\gamma = 0.47$, $k = 3.70 \cdot 10^3$, $\Lambda = 1.40 \cdot 10^{-4}$, for the inclined cable. These parameters correspond to a steel cable whose initial length is $L = 142.5\,\mathrm{m}$ for the first configuration whose span is $l = 130\,\mathrm{m}$, Young's effective modulus is $E = 100\,\mathrm{GPa}$; its cross-sectional area and moment of inertia are $A^0 = 8 \cdot 10^{-3}\,\mathrm{m}^2$ and $J^0 = 5.1 \cdot 10^{-6}\,\mathrm{m}^4$, respectively. The height of the inclined cable is $h = 30\,\mathrm{m}$ and its initial length is $L = 136.4\,\mathrm{m}$.

In all loading scenarios, we determine the cable response curves, depicting variations of the vertical displacement of a control point (point C whose arc length coordinate is $s = 1/3\,L$) with the magnitude of the force or support displacement. In particular, the loading path is discretized into N_L steps so that, by indicating with f_{N_L} the load magnitude at the end of the loading path and with f_j the magnitude at the jth step, we let $\alpha_j = f_j/f_{N_L}$ be the load multiplier. We monitored the configurations and state of stress at three given load steps, namely, $\alpha = 1/3, 2/3, 1$. For each of those three states, the tension, shear force, and flexural moment distributions along the cable are analyzed so as to point out the influence of the flexural rigidity throughout a comparison of the results with those obtained using the standard model that neglects the flexural stiffness.

5.1. Horizontal cable subject to an upward vertical load

The first case is that of a horizontal cable, shown in Figure 2, subject to an upward vertical load, distributed over a small region centered about the midspan whose length is $\Delta s = 0.1873\,\eta^0$. The nondimensional load amplitude is varied in the range $[0.03, 12]$. Because the force per unit reference length has been nondimensionalized with respect to mg/γ, and $\gamma = 1.5$; the maximum load is $f_{N_L} = 8\,mg$ and the resultant load becomes $F = 8\,mg(\Delta s\ell)$, which is about $3/2\,\mathrm{W}$, where $\mathrm{W} = mgL^0$ is the total weight of the cable. The loading process is discretized into $N_L = 400$ load steps with a resulting load step $\Delta f = 0.02993$.

The response curve in Figure 2 shows a softening behavior of the cable control point in both models. We further note that the curve representing the model with flexural stiffness is globally above the curve obtained with the standard cable model as it is to be expected since the cable with flexural stiffness is clearly stiffer than the purely extensible cable. This difference in behaviors is exhibited neither at the beginning nor at the end of the loading path whereas
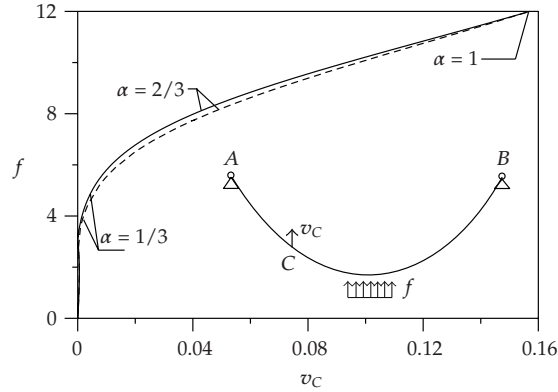
Figure 2: Response curves of the horizontal cable: variation of the vertical displacement of the control point *C* with the load magnitude obtained with the flexural stiffness (solid line) and without (dashed line).

the most prominent difference is appreciated when $\alpha = 2/3$, that is, when the upward load is nearly equal the weight of the cable.

Figure 3 shows the cable configurations at various load magnitudes, the initial static configuration $\mathcal{B}^0$ (catenary configuration), two intermediate configurations $\breve{\mathcal{B}}$ when $\alpha = 1/3$ ($F \simeq 1/2\,W$) and $\alpha = 2/3$ ($F \simeq W$) and the final configuration at the maximum load ($F \simeq 3/2\,W$). A region of negative curvatures is localized around the subdomain where the load is applied upward. In particular, when the load is between W and $3/2\,W$, the cable crosses the horizontal line passing through the supports and the extent of the central segment of the cable lifted above the horizontal line gradually increases up to the end of the loading path when it is nearly one third of the cable. At two thirds of the maximum load, the difference introduced by the flexural stiffness is quite remarkable especially if we consider the displacement of the midspan point around which we note appreciably different curvatures, sharper in the purely extensible cable. In Figure 4 (top), we show the tension along the cable whose evolution has two distinct phases. First, the application of the load tends to decrease uniformly the total tension in the cable until the load reaches a sufficient value to overcome the weight of the cable in the central region. At this stage, the curvature is reversed at the midspan and the tension gradually starts to exhibit sharp decreasing variations thus introducing a lack of uniformity of distribution. While at the midspan section the curvature (and the bending moment) increases, the tension tends to vanish; on the other hand, around the midspan, the tension has to balance part of the total weight of the cable. Concurrently, the shear load exhibits a boundary layer within the central loaded region, and the magnitude of the jump increases with the load amplitude. At the peak of the loading path, the bending moment is clearly localized within the central boundary layer with the peak moment being one order of magnitude higher than elsewhere in the cable.

5.2. Horizontal and inclined cables subject to support displacements

The right end boundary of the horizontal cable is moved horizontally to the left up to a nondimensional value of $u_B = 0.808$ (i.e., a dimensional displacement of the considered cable
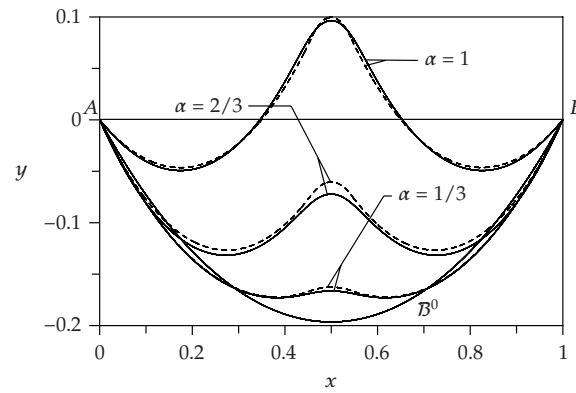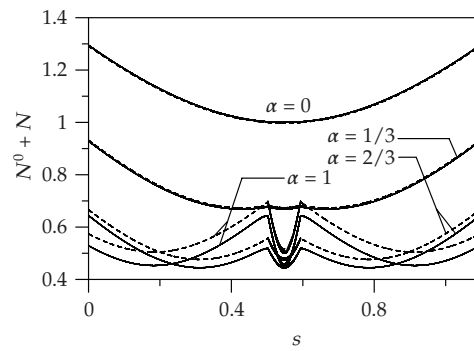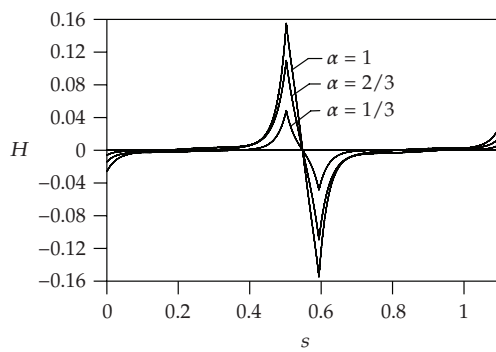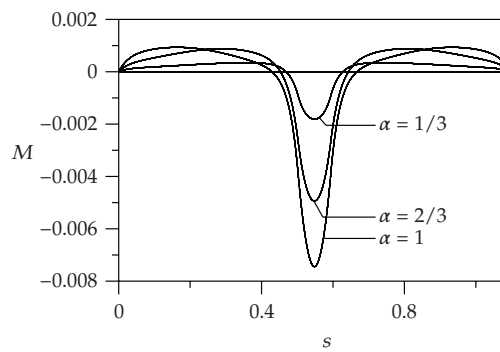
Figure 3: Cable configurations under an upward vertical load obtained with the flexural stiffness (solid lines) and without (dashed lines).

(a)

(b)

(c)

Figure 4: Tension (top), shear force (middle), and bending moments (bottom) of the cable under an upward vertical load obtained with the flexural stiffness (solid lines) and without (dashed lines).
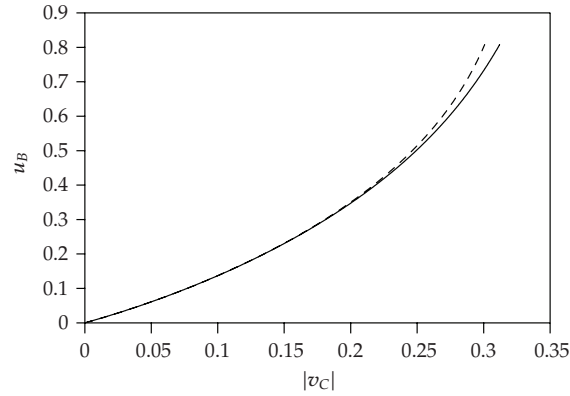
Figure 5: Response curves of the horizontal cable: variation of the vertical displacement of the control point C with the support displacement obtained with the flexural stiffness (solid line) and without (dashed line).
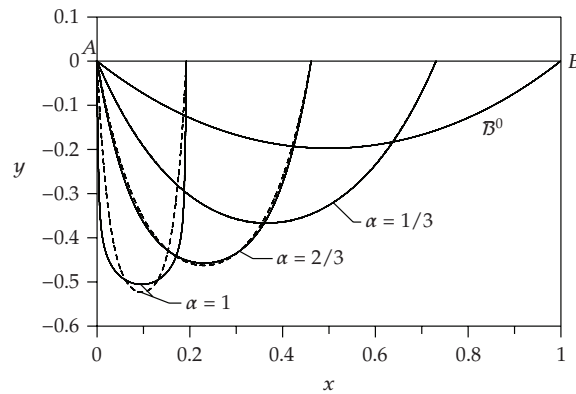

Figure 6: Cable configurations under a prescribed displacement of the support.

of 105 m) in $N_L = 1050$ steps. Figure 5 shows the response curve with the prescribed displacement u_B on the vertical axis and the displacement of the control point C on the abscissa axis. Besides, Figure 6 presents the configurations of both cables, with and without flexural stiffness, at the three load steps ($\alpha = 1/3, 2/3, 1$) and Figure 7 reports the associated tension, shear force, and bending moment.

During the whole loading path, a decrease of tension and an increase of shear force and bending moment are observed in the central region as the two boundaries are brought closer; further, as in the first loading scenario, the decrease becomes even more remarkable when the curvature is increasing. At the end of the loading path, the central region presents a tension that is almost close to zero bringing the cable close to a total loss of tension. Further, the shear force at the boundaries is appreciable. We also note that, as it has already been pointed out in previous studies, the standard model of purely extensible cables generates numerical instabilities when the tension levels are too low while the consideration of flexural
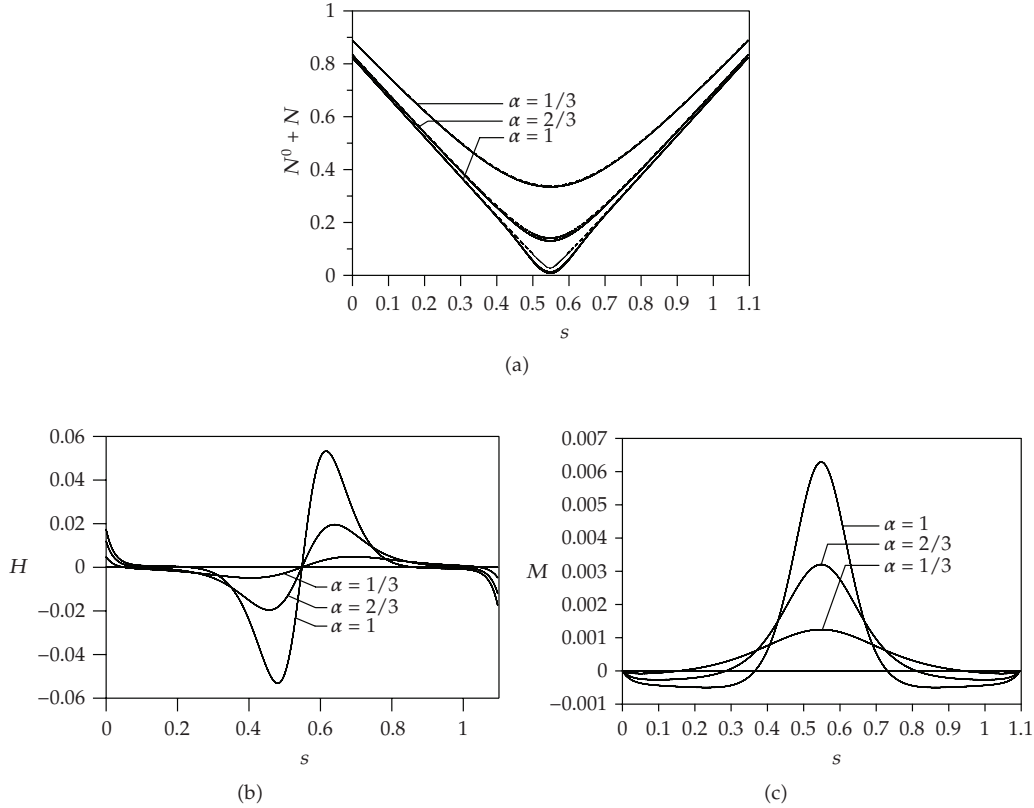
(a)

(b)

(c)

Figure 7: Tension (top), shear force (middle), and bending moments (bottom) of the cable subject to displacements of the support obtained with the flexural stiffness (solid lines) and without (dashed lines).

stiffness overcomes this problem. Moreover, the close observation of the differences in the configurations exhibited by the two cables reveals that the flexural stiffness has an appreciable influence on the equilibrium configuration even in the static regime, and points out the fact that it cannot be neglected in those segments of the cable where the tension is very low.

To quantify the differences in the state of stress, let us now consider the midspan section when $\alpha = 1$, and let $S = N/A^0$ denote the maximum tensile stress for the cable without flexural stiffness, and let $\overline{S} = \overline{N}/A^0 + \overline{M}/W_f^0$ be the tensile stress of the cable with flexural stiffness (where $W_f^0 = J^0/\sqrt{A/\pi}$ is the cable bending modulus). Calculating the relative percent difference between $\overline{S}$ and S yields a value about 53% which indicates that we would be led to underestimate the maximum tensile stress by the same amount with the standard cable model.

In the last loading scenario, the right support of the inclined cable is moved horizontally to the left up to a nondimensional value of $u_B = 0.769$ (i.e., a dimensional displacement of the considered cable of 100 m) in $N_L = 1000$ steps. Figure 8 shows the response curves whereas Figure 9 presents the configurations of both cables, with and without flexural stiffness, at the three load steps ($\alpha = 1/3, 2/3, 1$), and Figure 10 reports the associated tension, shear force, and
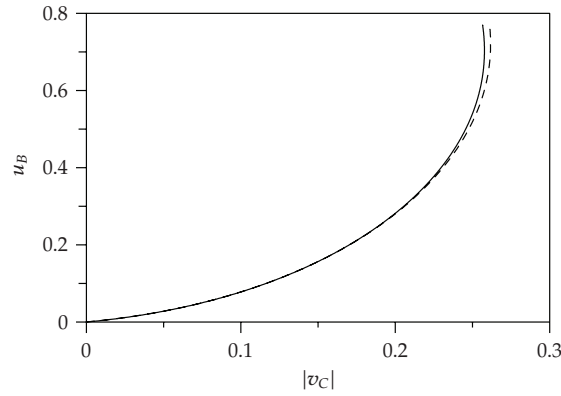
Figure 8: Response curves of the inclined cable: variation of the vertical displacement of the control point C with the support displacement obtained with the flexural stiffness (solid line) and without (dashed line).
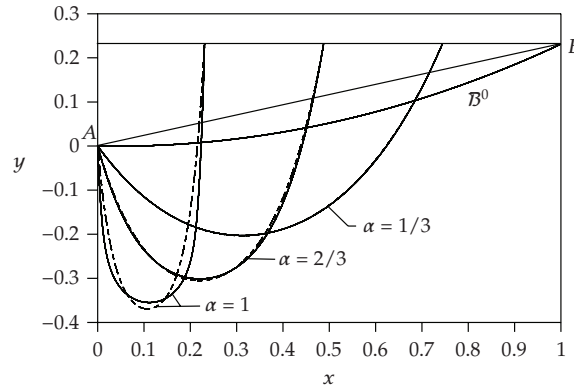

Figure 9: Cable configurations under a prescribed displacement of the support.

bending moment. This case is very similar to that of the horizontal cable although this cable is shallow and quite taut. The final maximum curvature is smaller than in the other case while the final lowest tension is bigger. It has to be noticed that, in this case, the most stressed region, on consideration of the shear force and flexural moment, is more shifted to the left due to the evident asymmetry of the problem.

6. Natural frequencies of cables with flexural stiffness

This section discusses concisely the vibration behavior of cables without flexural stiffness, in shallow and nonshallow regimes, with respect to the behavior of cables with flexural stiffness. To this end, variations of the lowest natural frequencies with Irvine's parameter λ are here reported. In Irvine's theory of shallow cables and in the generalized theory described in [5], the free motions of cables only depend on the two parameters (γ, λ) which completely
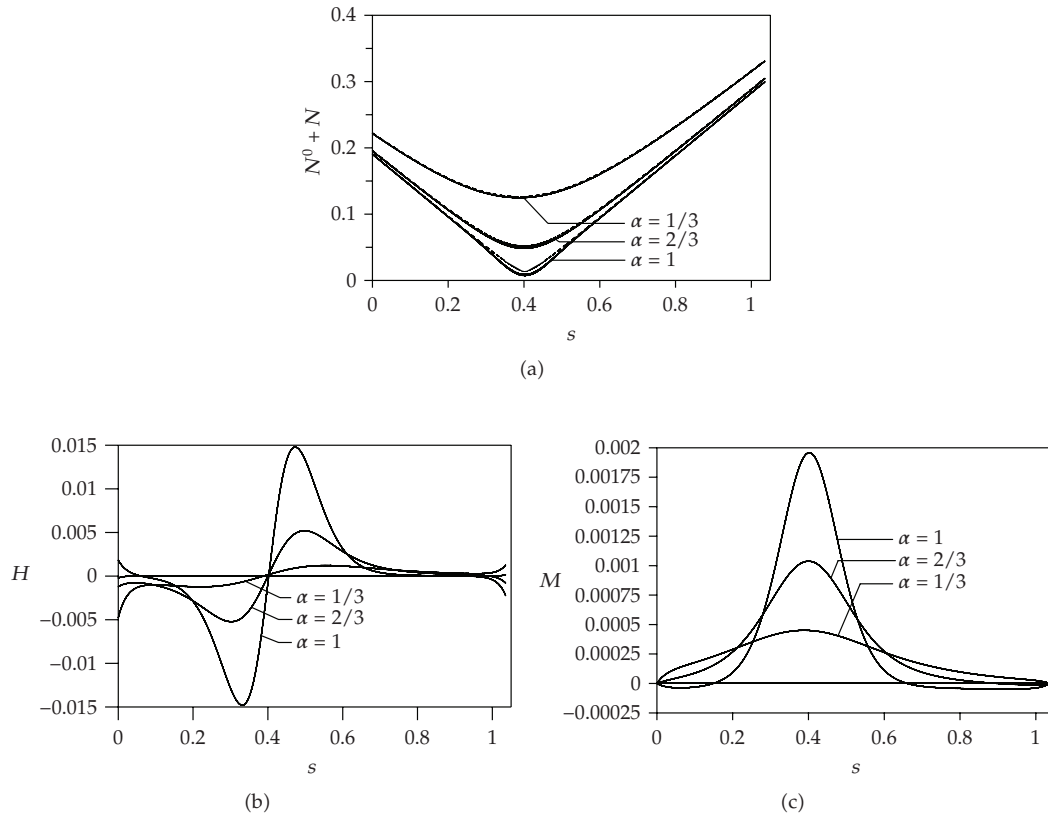
(a)

(b)

(c)

Figure 10: Tension (top), shear force (middle), and bending moments (bottom) of the cable subject to displacements of the support obtained with the flexural stiffness (solid lines) and without (dashed lines).

characterize the geometric and elastic properties of linearly elastic cables. Taking into account the flexural stiffness introduces a new elastogeometric parameter, Λ. In Figure 11, variations of the lowest natural frequencies with λ/π are shown as obtained with the two relevant models, with incorporation of the flexural stiffness (solid lines) and without flexural stiffness (dashed lines). We consider three different regimes: shallow cables with $\gamma = 0.1$, transition cables with $\gamma = 0.75$, and nonshallow cables with $\gamma = 1.5$. In Figure 11 (top), in the case of shallow cables ($\gamma = 0.1$), differences between the two models are not easily detectable except mild differences for $\lambda > 0.7\pi$. On the other hand, for nonshallow cables ($\gamma = 1.5$), we clearly observe a deviation of the loci of the eigenfrequencies to higher values with increasing λ. As a matter of a fact, flexural stiffness effects are expected to be more significant for cables with larger cross-section areas, that is, in our case, those corresponding to larger values of λ. Here, the assumed data are γ (that defines the geometric stiffness) and E, Young's modulus. At the same time, higher modes present a number of curvature variations, hence a number of nodes, greater than the lower modes so that the flexural rigidity is expected to impact the frequencies of the higher modes as it can be seen in Figure 11. Furthermore, the increase of the natural frequencies due to the flexural stiffness effects do not seem to generate new crossovers.
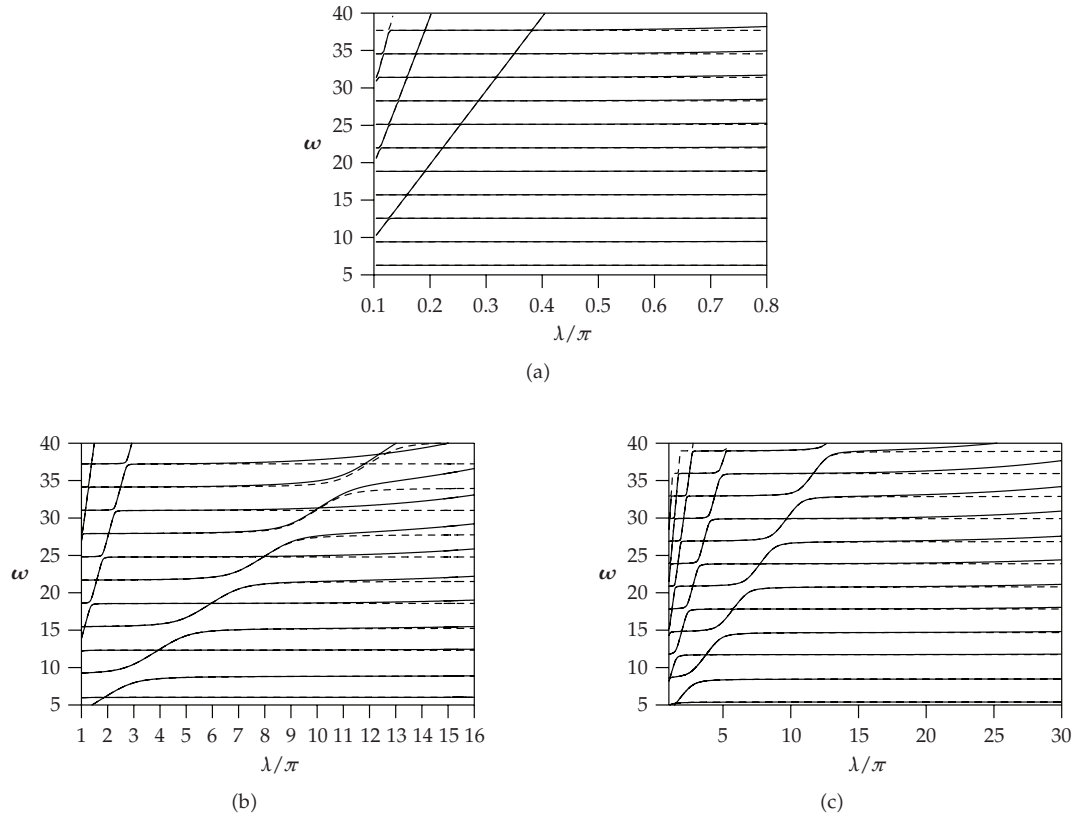
(a)

(b)

(c)

Figure 11: Variation of the lowest natural frequencies with λ/π obtained with the flexural stiffness (solid lines) and without (dashed lines) when $\gamma = 0.1, 0.75, 1.5$, respectively.

7. Concluding remarks

A geometrically exact formulation of cables undergoing axis stretching and flexural curvature has been proposed. The model, in its general form, is suitable to treat more general cable regimes, such as the loosening regime whereby a local loss of tension occurs.

The equations of motion have been formulated for cables with nonlinearly viscoelastic constitutive laws and general loading conditions. The particular case of cables with a linearly elastic constitutive law has been then considered in the numerical calculations conducted on horizontal and inclined cables by employing a path-following scheme with two different discretizations: a finite-difference approach and a finite element formulation. In particular, low-tension regimes have been investigated, and the flexural stiffness influence on shallow and nonshallow cable behaviors has been studied outlining its importance in the structural response in the mentioned low-tension regime.

The most remarkable loading case, presented in this paper, is relative to a displacement of the right support moved toward the left support. It has been shown that an underestimation of the maximum tensile stress of about 50% would be reached were we to employ the crude model of purely extensible cables. Although the probability of such a phenomenon is

low in civil engineering applications since the displacements are expected to be small, the extreme scenarios here reproduced can certainly concern mooring cables or cables in tethered space applications. In addition, consideration of the flexural stiffness is important to correctly evaluate the fatigue life of cables.

Modeling linearly elastic cables with flexural stiffness has led to a new independent parameter, denoted Λ, which represents the ratio between the flexural and the geometric stiffnesses. The presence of flexural stiffness modifies the loci of the higher frequencies at higher stiffnesses, especially in nonshallow cables.

More in-depth investigations are needed to correctly unfold the cables behavior near instabilities or in the fully developed post-critical scenarios (galloping, parametric reso-nance,..., etc.) whereby loosening phenomena and nonlinear viscoelasticity within the boundary layers are expected to play a critical role on the response.

Appendix

The static configuration $\mathcal{B}^0$

The static configuration under the cable own weight is obtained integrating (2.8) with the inex-tensibility constraint $\nu^0 = 1$ which yields $\sigma = s$. By introducing the following nondimensional variables and parameters:

$$\gamma = \frac{mg\ell}{H^0}, \qquad \beta = \frac{mg\ell}{V^0}, \tag{A.1}$$

and integrating the equilibrium equations yields

$$x(s) = \frac{1}{\gamma}\left[\sinh^{-1}\left(\frac{\gamma}{\beta} + \gamma s\right) - \sinh^{-1}\left(\frac{\gamma}{\beta}\right)\right],$$

$$y(s) = \frac{1}{\gamma}\left[\sqrt{1 + \left(\frac{\gamma}{\beta} + \gamma s\right)^2} - \sqrt{1 + \left(\frac{\gamma}{\beta}\right)^2}\right], \tag{A.2}$$

where H^0 is the horizontal projection of the tension at the left support, the star was dropped, and $\sinh^{-1}$ denotes the inverse function of sinh. The boundary conditions give two transcendental equations in the unknowns γ and β. For instance, for horizontal cables, the compatibility condition becomes

$$\eta^0 \frac{\gamma}{2} = \sinh\left(\frac{\gamma}{2}\right). \tag{A.3}$$

Typically, η^0 is known (the initial cable length as well as the span), hence the compatibility equation is solved for γ. On the other hand, in the case of inclined cables, imposing the boundary conditions yields the following transcendental equations:

$$\sqrt{1 + \left(\frac{\gamma}{\beta} + \gamma\eta^0\right)^2} - \sqrt{1 + \left(\frac{\gamma}{\beta}\right)^2} = \frac{\gamma h}{\ell},$$

$$\frac{1}{\gamma}\left[\sinh^{-1}\left(\frac{\gamma}{\beta} + \gamma\eta^0\right) - \sinh^{-1}\left(\frac{\gamma}{\beta}\right)\right] = 1. \tag{A.4}$$

Acknowledgment

References

[1] H. M. Irvine, *Cables Structures*, Dover, New York, NY, USA, 1984.

[2] A. Luongo, G. Rega, and F. Vestroni, Planar nonlinear free vibrations of an elastic cable, *International Journal of Non-Linear Mechanics*, vol. 19, no. 1, pp. 3952, 1984.

[3] G. Rega, W. Lacarbonara, A. H. Nayfeh, and C. M. Chin, Multiple resonances in suspended cables: direct versus reduced-order models, *International Journal of Non-Linear Mechanics*, vol. 34, no. 5, pp. 901924, 1999.

[4] G. Rega, Nonlinear vibrations of suspended cables—part II: deterministic phenomena, *Applied Mechanics Reviews*, vol. 57, no. 6, pp. 479514, 2004.

[5] W. Lacarbonara, A. Paolone, and F. Vestroni, Elastodynamics of nonshallow suspended cables: linear modal properties, *Journal of Vibration and Acoustics*, vol. 129, no. 4, pp. 425433, 2007.

[6] W. Lacarbonara, A. Paolone, and F. Vestroni, Nonlinear modal properties of non-shallow cables, *International Journal of Non-Linear Mechanics*, vol. 42, no. 3, pp. 542554, 2007.

[7] J. J. Burgess, Bending stiffness in a simulation of undersea cable deployment, *International Journal of Offshore and Polar Engineering*, vol. 3, no. 3, pp. 197204, 1993.

[8] M. S. Triantafyllou and C. T. Howell, Dynamic response of cables under negative tension: an ill-posed problem, *Journal of Sound and Vibration*, vol. 173, no. 4, pp. 433447, 1994.

[9] Y. Sun and J. W. Leonard, Dynamics of ocean cables with local low-tension regions, *Ocean Engineering*, vol. 25, no. 6, pp. 443463, 1998.

[10] Y. Q. Ni, J. M. Ko, and G. Zheng, Dynamic analysis of large-diameter sagged cables taking into account flexural rigidity, *Journal of Sound and Vibration*, vol. 257, no. 2, pp. 301319, 2002.

[11] Y. T. Chai, K. S. Varyani, and N. D. P. Barltrop, Three-dimensional Lump-Mass formulation of a catenary riser with bending, torsion and irregular seabed interaction effect, *Ocean Engineering*, vol. 29, no. 12, pp. 15031525, 2002.

[12] Q. Wu, K. Takahashi, and S. Nakamura, The effect of cable loosening on seismic response of a prestressed concrete cable-stayed bridge, *Journal of Sound and Vibration*, vol. 268, no. 1, pp. 7184, 2003.

[13] Q. Wu, K. Takahashi, and S. Nakamura, Nonlinear vibrations of cables considering loosening, *Journal of Sound and Vibration*, vol. 261, no. 3, pp. 385402, 2003.

[14] Q. Wu, K. Takahashi, and S. Nakamura, Nonlinear response of cables subject to periodic support excitation considering cable loosening, *Journal of Sound and Vibration*, vol. 271, no. 1-2, pp. 453463, 2004.

[15] Q. Wu, K. Takahashi, and B. Chen, Influence of cable loosening on nonlinear parametric vibrations of inclined cables, *Structural Engineering & Mechanics*, vol. 25, no. 2, pp. 219237, 2007.

[16] S. S. Antman, *Nonlinear Problems of Elasticity*, vol. 107 of *Applied Mathematical Sciences*, Springer, New York, NY, USA, 2nd edition, 2005.

[17] L. Fox, *The Numerical Solution of Two-Point Boundary Problems in Ordinary Differential Equations*, Oxford University Press, New York, NY, USA, 1957.

[18] MATHEMATICA, 2007, Wolfram Research Inc., Urbana Champaign, Ill, USA.

[19] COMSOL, 2005, Comsol Multiphysics Inc., Stokholm, Sweden.